Giant *meso–meso*-Linked Porphyrin Arrays of Micrometer Molecular Length and Their Fabrication

Naoki Aratani,[a] Akihiko Takagi,[b] Yoshiki Yanagawa,[b] Takuya Matsumoto,*[b] Tomoji Kawai,*[b] Zin Seok Yoon,[c] Dongho Kim,*[c] and Atsuhiro Osuka*[a]

Abstract: On the basis of the Ag^{I}-promoted coupling reaction of zinc(II)–5,15-bis(3,5-dioctyloxyphenyl)porphyrin **Z1**, chain elongation has been attempted by using a stepwise doubling approach, which provides **Z2**, **Z4**, **Z8**, **Z16**, **Z32**, **Z64**, **Z128**, **Z256**, **Z384**, and **Z512**. The porphyrin arrays up to **Z128** are sufficiently soluble in $CHCl_3$ and THF despite their very long molecular lengths and rodlike structures, while the arrays over **Z128** show a significant drop in solubility and stability. The discrete porphyrin arrays thus isolated were characterized by means of ^{1}H NMR spectroscopy, matrix-assisted laser desorption ionization time-of-flight (MALDI-TOF) mass spectrometry, UV/Vis spectroscopy, gel-permeation chromatography (GPC), cyclic voltammetry (CV), single-crystal X-ray crystallography, scanning tunneling microscopy (STM), and atomic force microscopy (AFM). Contrary to expected linear conformations of the arrays **Z*n*** (where *n* is the number of porphyrins), the single molecular images of **Z128**, **Z256**, and **Z512** revealed largely bent structures; this finding indicates the substantial conformational flexibility of **Z*n***. We also exploited an effective synthetic route by means of which **Z*n*** can be fabricated with a thiol-protected aryl group to provide $\mathbf{Z}n\mathbf{S}_2$ through $\mathbf{Z}n\mathbf{Br}_2$, by bromination with *N*-bromosuccinimide and subsequent Pd-catalyzed Suzuki–Miyaura arylation. Finally, the reaction of **Z256** provided **Z512**, **Z768**, and **Z1024**. Collectively, this work provides an important milestone in the preparation of sub-microscale discrete organic molecules and the fabrication of molecular-based materials, hence significantly contributing to device applications.

Keywords: C–C coupling · cross-coupling · nanostructures · oligomerization · porphyrinoids

Introduction

In the last two decades, remarkable progress has been made in the synthesis of electrochemically and/or photochemically active oligomeric and polymeric materials, which has led to the exploration of new molecular architectures, better understanding of their properties, and practical applications in electronic and optical devices.[1–7] Even though both the theories and calculations have been explored based on ideal polymers,[8] experiments on monodisperse oligomers, in which no ensemble averaging is needed, can provide more direct and insightful information and are thus of great im-

[a] Dr. N. Aratani, Prof. Dr. A. Osuka
Department of Chemistry, Graduate School of Science
Kyoto University, Sakyo-ku, Kyoto 606–8502 (Japan)
Fax: (+81) 75-753-3970
E-mail: osuka@kuchem.kyoto-u.ac.jp

[b] Dr. A. Takagi, Y. Yanagawa, Prof. Dr. T. Matsumoto, Prof. Dr. T. Kawai
The Institute of Scientific and Industrial Research (ISIR)
Osaka University, 8–1, Mihogaoka, Ibaraki 567–0047 Osaka (Japan)
Fax: (+81) 66-875-2440
E-mail: matsumoto@sanken.osaka-u.ac.jp
kawai@sanken.osuka-u.ac.jp

[c] Z. S. Yoon, Prof. Dr. D. Kim
Center for Ultrafast Optical Characteristics Control and Department of Chemistry
Yonsei University, Seoul 120–749 (Korea)
Fax: (+82) 22-123-2434
E-mail: dongho@yonsei.ac.kr

Supporting information for this article is available on the WWW under http://www.chemeurj.org/ or from the author. Synthetic procedures for the new compounds, the recycling GPC chromatograms for the separation of the **Z8** reaction mixture, ROESY ^{1}H NMR spectrum of **Z4**, ^{1}H NMR spectra of **H*n***, ESR spectrum of the radical cation of zinc(II)–5,15-bis(3,5-di-*tert*-butylphenyl)porphyrin complex formed by electrochemical oxidation, and UV/Vis absorption and fluorescence data of **Z*n***.

 DOI: 10.1002/chem.200401306

portance. In this context, the synthesis of monodisperse macromolecular rods of precise length and constitution has attracted keen attention in light of their potential application in molecular-scale electronics, optical devices, solar energy conversion, and so forth,[1–3] because such discrete oligomers can also offer a good opportunity for systematic studies on structure–property relationships that will be useful for predicting specific electronic, photonic, and morphological property data.

Through recent extensive synthetic efforts, the range of molecular lengths of linear monodisperse π-conjugated oligomers has now reached over 10 nm. With respect to oligo-*p*-phenylene, up to 16 *p*-phenylene rings were covalently connected by use of the repetitive approach by Hensel and Schlüter,[9] who also synthesized a cyclotetraicosaphenylene based on the same strategy.[10] Meier et al. synthesized monodisperse oligo(1,4-phenylene ethenylene)s up to 12-mer as a more planar π-conjugated oligomer.[11] Tour et al. developed an approach to growing molecular systems by means of an iterative divergent/convergent method, which resulted in the synthesis of phenylethynyl 18-mer bearing protected thiol groups for connection onto gold electrodes.[12] This method, when combined with solid-phase synthesis, furnished a block-alternating 23-mer consisting of oligo(1,4-phenylene ethynylene)s and oligo(2,5-thiophene ethynylene)s, the molecular length of which reached about 160 Å.[13]

Conversely, oligo- and polythiophenes have been actively exploited for molecular devices, such as organic conductive materials, electroluminescence (EL) devices, organic light-emitting diodes (OLEDs), field-effect transistors (FETs), and so forth.[14–17] Roncali et al. reported the synthesis and characterization of monodisperse soluble oligothienylenevinylenes with chain lengths up to 10 nm.[15] A series of long discrete oligothiophene molecules was synthesized by Otsubo and co-workers,[17] whose work culminated in the synthesis of a discrete 96-mer.[17a] Yet it still remains as a great synthetic challenge to explore discrete functional molecules with well-defined structures far beyond the above achievements.

Among the molecular modules suitable for use as a construction element of supramolecular rods, porphyrins are one of the most attractive building blocks, because they offer a variety of desirable features, such as rigid planar geometry, high stability, intense electronic absorption and emission, a small HOMO–LUMO energy gap, and flexible tunability of their optical and redox properties by appropriate metalation.[18] In fact, extensive efforts have been made to prepare porphyrin arrays with a view to their use in realizing various functional units and molecular devices.[19] However, these studies have often been hampered by poor solubility, difficult separation, and demanding characterization, all of which are intrinsic problems of covalently linked, large porphyrin arrays.

Recently, we reported the Ag^{I}-promoted *meso–meso* coupling reaction of a Zn^{II}–5,15-diarylporphyrin.[20,21] This reaction has the following advantages: 1) the regioselectivity of the *meso–meso* coupling reaction is always quite high, 2) the molecular length grows rapidly at the rate of 2^n, where n is the number of iterations, 3) the orthogonal conformations of the porphyrin array products causes them to be highly soluble, which allows the manipulation of very long porphyrin arrays, 4) the separation of the coupling products is easily carried out by means of recycling preparative gel-permeation chromatography HPLC (GPC-HPLC), due to the large difference in the molecular weights of the porphyrin products, and finally 5) the long coupling products still bear two free *meso*-positions that are available for the next reaction as long as the porphyrin array is soluble in the reaction solvent. Taking advantage of these features, we synthesized a series of *meso–meso*-linked porphyrin arrays up to 128-mer, which was, at that time, the longest discrete molecule made.[1j,20b] In this respect, further extension of this synthetic strategy is challenging in its own right.

Here, we report the synthesis of a series of much longer *meso–meso*-linked porphyrin arrays. These arrays are particularly attractive due to their linear rodlike structure, ample electronic interaction between neighboring porphyrins, and unprecedented giant molecular size. These properties are interesting from a photonic-molecular-wire viewpoint, because 1) the large Coulombic interactions between the neighboring porphyrins are favorable for rapid excitation energy hopping,[22] and 2) each porphyrin unit retains its individual character, presumably because of the orthogonal geometry, thus preventing the formation of an energy sink.[23] Moreover, it has been demonstrated that these porphyrin arrays can be effectively transformed into completely π-conjugated, fused porphyrin arrays, which exhibit an extremely low optical HOMO–LUMO gap, down to approximately 0.16 eV at the stage of 12-mer, and hence, encouraging the potential conversion of a photonic wire to an electronic wire.[24]

To use these porphyrin arrays in a variety of applications, it is highly desirable to fabricate them with a thiol or carboxylic acid group, which will allow a chemical bond to be formed between the array and a metal surface. In this respect, the free end *meso*-position of the *meso–meso*-linked porphyrin arrays is quite attractive. Thus, we examined the reactivity of the end *meso*-position and developed a useful and complete conversion into *meso*-mercaptophenylporphyrin arrays.

In the present study, we isolated a *meso–meso* linked porphyrin 1024-mer, which is, to the best of our knowledge, the longest (ca. 850 nm = 0.85 μm) monodisperse rodlike man-made molecule,[1j] which has a molecular formula of $C_{65536}H_{83970}N_{4096}O_{4096}Zn_{1024}$.

Results

Synthesis and separation: *meso–meso*-Coupled porphyrin oligomers were prepared by the Ag^{I}-promoted oxidative coupling reaction.[20] One of the key advantages of this synthetic strategy is the high solubility of long porphyrin prod-

ucts, even in their 128-mer stage, which allows for their isolation and characterization. The synthesis of zinc(II)–5,15-bis(3,5-dioctyloxyphenyl)porphyrin (**Z1**) is shown in Scheme 1. 3,5-Dihydroxybenzoic acid (**1**) was esterified in

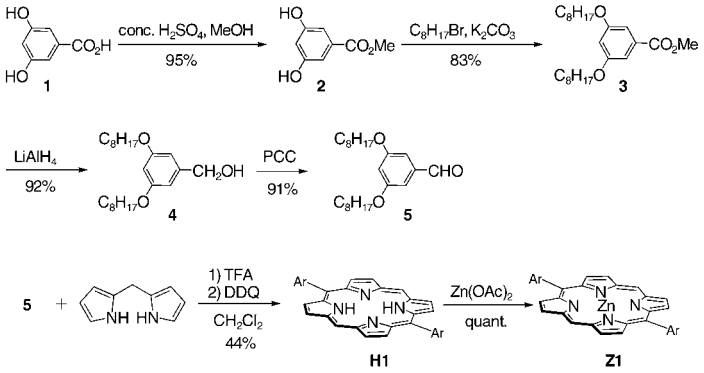

Scheme 1. Synthesis of **Z1**. Ar = 3,5-dioctyloxyphenyl.

methanol with a catalytic amount of concentrated H_2SO_4 to form methyl 3,5-dihydroxylbenzoate (**2**). Alkylation of the ester **2** was performed by a Williamson-type reaction to give methyl 3,5-dioctyloxybenzoate (**3**), which was reduced with $LiAlH_4$ to 3,5-dioctyloxybenzyl alcohol (**4**). 3,5-Dioctyloxybenzaldehyde (**5**) was obtained by oxidation of **4** with pyridinium chlorochromate in CH_2Cl_2. The porphyrin **Z1** was prepared from **5** and bis(2-pyrryl)methane (**6**)[25] in 44% yield under the standard conditions.[26]

The chain elongation strategy is quite simple, that is, by repeating dimerization reactions from **Z1** to **Z2**, **Z2** to **Z4**, **Z4** to **Z8**, **Z8** to **Z16**, **Z16** to **Z32**, **Z32** to **Z64**, and **Z64** to **Z128** (Scheme 2). The reaction of **Z1** with $AgPF_6$ (1.2 equiv in $CHCl_3$) at 30°C for 10 h, followed by preparative SEC (size-exclusion chromatography) gave **Z2** (22–27%), **Z3** (3–6%), **Z4** (2%), and a small amount of higher oligomers along with the recovery of **Z1** (50–55%). In each step, dimerized, trimerized, and tetramerized compounds were obtained constantly in 20–30%, ~13%, and ~6% yields, respectively, along with the recovery of starting materials (50–55%). Use of purified $CHCl_3$ as the reaction solvent and keeping the reaction temperature strictly at 30°C were crucial to attaining constant results, because the coupling reaction of **Z1** is sensitive to additives and temperatures. Addition of small amounts (0.5–3%) of *N,N*-dimethylformamide (DMF), *N,N*-dimethylacetamide (DMA), or hexamethylphosphoramide (HMPA) accelerated the reaction to give poly(Zn^{II}–porphyrinylene),[27] while addition of small amounts of amine resulted in complete retardation of the coupling reaction.[28] Slight heating (40–50°C) also accelerated the coupling reaction to provide a wider range of large porphyrin arrays in an uncontrollable manner.

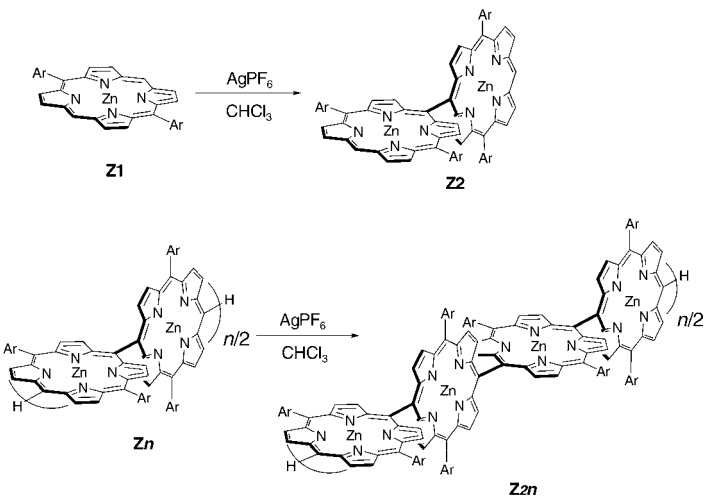

Scheme 2. Synthesis of **Z*n***. Ar = 3,5-dioctyloxyphenyl.

The use of recycling preparative GPC-HPLC was crucial for the isolation of porphyrin products. Figure 1 shows GPC-HPLC chromatographs (column conditions: JAI-GEL 5H-AF, 4H-AF, and 3H-AF with THF) of the reactions of **Z1**, **Z2**, **Z4**, and **Z8** (Figure 1 left), **Z16**, **Z32**, and **Z64** (Figure 1 right). The coupling products were nicely separated by means of GPC-HPLC in all cases, after several recycling separations owing to large differences in molecular weight, thus allowing isolation of pure, long porphyrin arrays. In each step, strict separation of the doubling product is crucially important for further chain elongation, as even a small amount of contamination will lead to serious problems in the longer array. During many repeated preparations, we also isolated **Z3**, **Z5**, **Z6**, **Z7**, **Z10**, **Z12**, **Z20**, **Z24**, **Z40**, **Z48**, **Z80**, **Z96**, and **Z192**, and accumulated more than 100 mg of **Z128**.

Additionally, **Z*n*** can be transformed into the corresponding free-base porphyrin arrays **H*n*** (where *n* represents the number of porphyrins) in good yields, which can in turn be metalated with a variety of metal ions to give metalated *meso–meso*-linked arrays.

The **Z128** array has a molecular length of about 106 nm in its linear form, but is sufficiently soluble in THF and $CHCl_3$. Thus, the coupling reaction of **Z128** was attempted, although the coupling reaction of such an extremely long molecule should be entropically very unfavorable because of only two reactive free *meso*-positions. **Z128** was reacted with $AgPF_6$ (12 equiv in $CHCl_3$) for 11 h at room temperature, and the reaction mixture was analyzed by GPC-HPLC, which indicated the formation of **Z256**, **Z384**, and **Z512** (Figure 2 left). These large porphyrin arrays were actually isolated by the preparative recycling GPC-HPLC in yields of 26, 11, and 4%, respectively. Isolated arrays eluted at 14.8 min (**Z256**), 14.1 min (**Z384**), and 13.6 min (**Z512**) on the present column setup. While **Z128** can be stored in a refrigerator for a long time without serious deterioration and can be manipulated essentially in a similar manner to normal, small organic compounds, the manipulation of the larger arrays (**Z256**, **Z384**, and **Z512**) is more difficult, because, although freshly separated samples are reasonably soluble, they change to an insoluble material even upon storage in a refrigerator in the dark. Once these porphyrin arrays become insoluble, it is

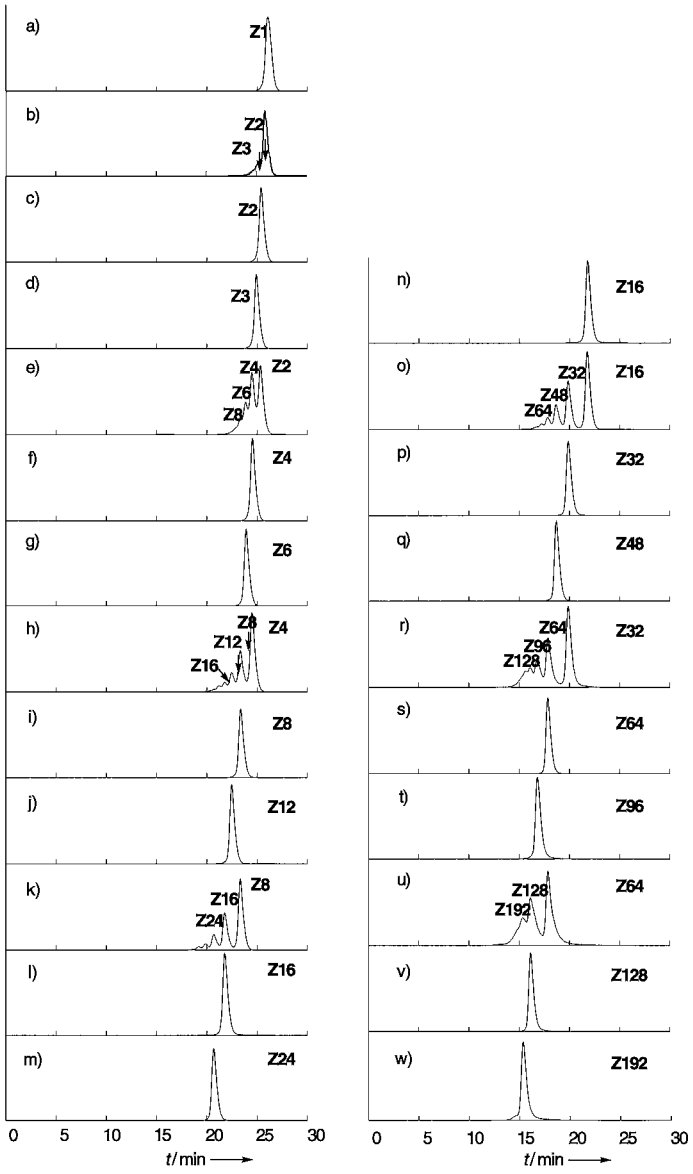

Figure 1. GPC-HPLC chromatograms of the Ag^{I}-promoted coupling reaction detected by absorbance at 413 nm. Each chromatogram is normalized to the maximum intensity. Left: The reaction a–d) from **Z1**, e–g) from **Z2**, h–j) from **Z4**, and k–m) from **Z8**; a) **Z1**, b) after 9 h, c) purified **Z2**, d) purified **Z3**, e) after 8 h, f) purified **Z4**, g) purified **Z6**, h) after 4 h, i) purified **Z8**, j) purified **Z12**, k) after 8 h, l) purified **Z16**, and m) purified **Z24**. Right: The reaction n–q) from **Z16**, r–t) from **Z32**, and u–w) from **Z64**; n) **Z16**, o) after 9 h, p) purified **Z32**, q) purified **Z48**, r) after 8 h, s) purified **Z64**, t) purified **Z96**, u) after 11 h, v) purified **Z128**, and w) purified **Z192**. The GPC column setup is the combination of JAI-GEL 5H-AF, 4H-AF, and 3H-AF.

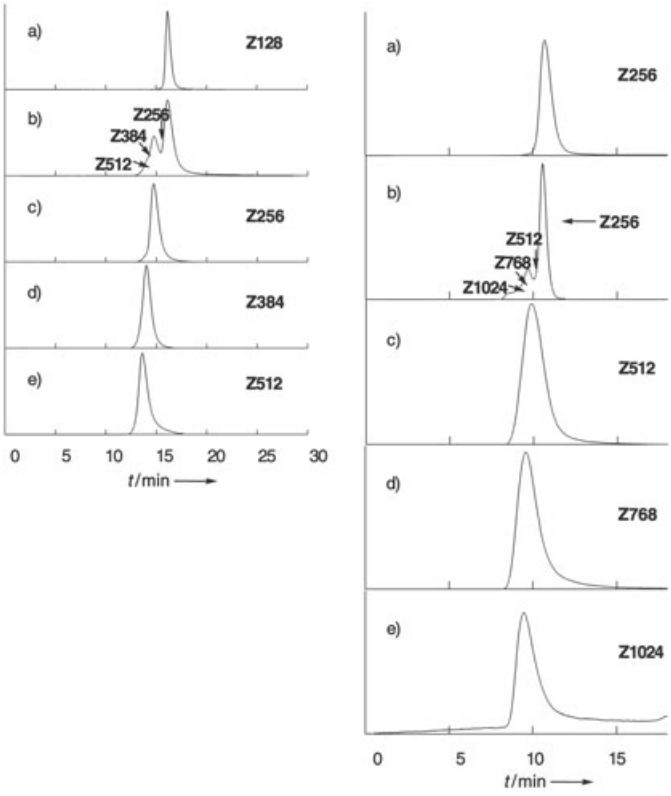

Figure 2. Left: GPC-HPLC chromatograms of the reaction from **Z128**: a) **Z128**, b) reaction mixture of **Z128**, c) purified **Z256**, d) purified **Z384**, and e) purified **Z512**. The GPC setup is the combination of JAI-GEL 5H-AF, 4H-AF, and 3H-AF. Right: GPC-HPLC chromatograms of the reaction from **Z256**: a) **Z256**, b) reaction mixture of **Z256**, c) purified **Z512**, d) purified **Z768**, and e) purified **Z1024**. The GPC column setup is the combination of JAI-GEL 5H-AF and 4H-AF.

very difficult to redissolve them in common organic solvents. This tendency becomes more serious upon increasing the array size.

Finally, we examined the coupling reaction of **Z256** under similar conditions. If this trial were to go well, the longest molecule would be formed. Actually this attempt afforded **Z512**, **Z768**, and **Z1024**, as judged from the GPC-HPLC chart of the reaction mixture (Figure 2 right). We used a different analytical column setup to get better separation for larger arrays: JAI-GEL 5H-AF and 4H-AF with THF. The preparative GPC column showed clearer separation (Figure 3). These reaction products were separated with

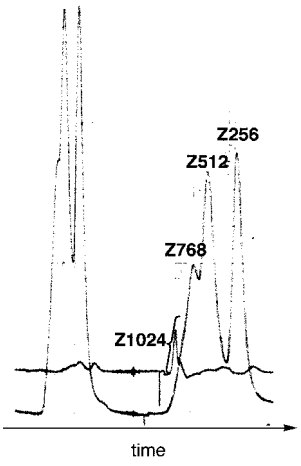

Figure 3. Preparative GPC-HPLC chromatogram of the reaction from **Z256**.

considerable difficultly, because their retention times are quite close to the exclusion limit. But after repeated recycling separations over the preparative GPC-HPLC, we isolated **Z512** (13%), **Z768** (5%), and **Z1024** (2%). These isolated long arrays exhibited the retention times of 9.9, 9.6, and 9.5 min, respectively. The longest molecule, **Z1024**, has a molecular length of 0.85 μm in its linear form and a molecular formula of $C_{65536}H_{83970}N_{4096}O_{4096}Zn_{1024}$.

The molecular weights of these porphyrin arrays, up to **Z128**, were carefully determined by matrix-assisted laser desorption ionization time-of-flight (MALDI-TOF) mass spectrometry, and the results are summarized in Table 1. The mass spectra of **Z64**, **Z96**, and **Z128** revealed the parent peaks at 66323, 99050, and 130295, respectively, along small dicationic peaks, clearly indicating their clean monodispersity (Figure 4). Unfortunately, however, the parent ion peaks of porphyrin arrays higher than **Z128** could not be detected.

Further information on the monodispersity of the separated porphyrin arrays was given from their GPC-HPLC eluting features, as all of the isolated porphyrin arrays exhibited clear elution bands on the GPC-HPLC charts, and their retention times showed a good continuous relationship, similar to that of polystyrene standards, versus the actual molecular weights. **Z*n*** arrays and polystyrene standards eluted in a similar manner against their molecular weights in the $\log M_w < 4$ region, while **Z*n*** arrays eluted much faster than polystyrene standards of the same molecular weight in the $\log M_w > 4$ region, and this discrepancy became more significant with increasing molecular weight (Figure 5a). Figure 5b demonstrates the good continuous relationship of the actual molecular weights versus analytical GPC molecular weights estimated with respect to polystyrene standards.

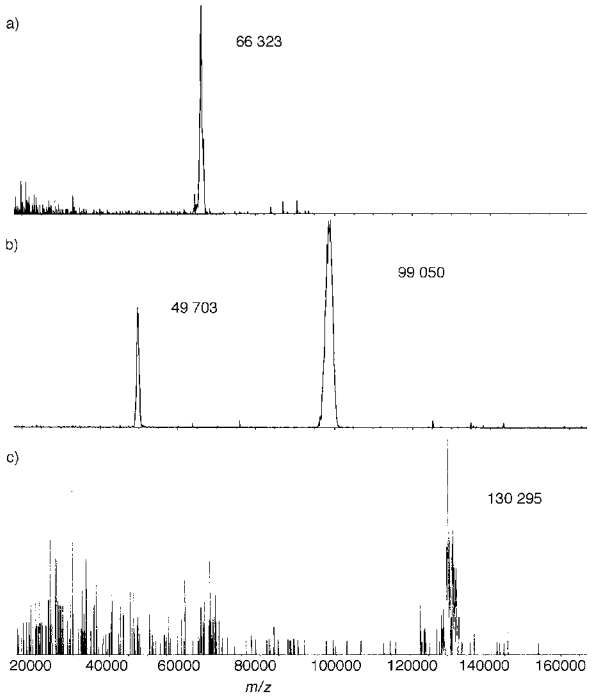

Figure 4. MALDI-TOF mass spectra (9-nitroanthracene was used as a matrix). a) **Z64**, b) **Z96**, and c) **Z128**.

^{1}H NMR spectroscopy: ^{1}H NMR spectra of **Z1**–**Z8**, taken in $CDCl_3$ at room temperature, are shown in Figure 6. Assignments were performed by means of comprehensive ROESY experiments (the designation of the protons is given in Scheme 3. See also Supporting Information). In the spectrum of **Z1**, a singlet for the *meso* protons (H^m) appears at 10.31 ppm and two doublets for the β protons appear at 9.43 (H^1) and 9.26 ppm (H^2). The spectrum of **Z2** exhibits a singlet for H^m at 10.38 ppm, two doublets for the outer β protons at 9.49 and 9.28 ppm (H^1 and H^2, respectively), and two doublets for the inner β protons at 8.82 (H^3) and 8.10 ppm (H^4), which are characteristic of a *meso–meso*-linked diporphyrin. The inner β protons are lying in the shielding region of the neighboring porphyrin. Similarly, the spectrum of **Z3** exhibits a singlet for H^m, two doublets for H^1 and H^2, and four dou-

Table 1. **Z*n*** compounds list. Observed and calculated molecular weights and GPC retention times [min].

Compound	Molecular formula	M_c[a]	M_o[b]	Retention time[c]
Z1	$C_{64}H_{84}N_4O_4Zn$	1037	1036	26.1
Z2	$C_{128}H_{166}N_8O_8Zn_2$	2075	2076	25.4
Z3	$C_{192}H_{248}N_{12}O_{12}Zn_3$	3114	3112	24.9
Z4	$C_{256}H_{330}N_{16}O_{16}Zn_4$	4146	4145	24.5
Z5	$C_{320}H_{412}N_{20}O_{20}Zn_5$	5186	5183	24.2
Z6	$C_{384}H_{494}N_{24}O_{24}Zn_6$	6222	6214	23.9
Z7	$C_{448}H_{576}N_{28}O_{28}Zn_7$	7259	7253	23.6
Z8	$C_{512}H_{658}N_{32}O_{32}Zn_8$	8296	8286	23.4
Z10	$C_{640}H_{822}N_{40}O_{40}Zn_{10}$	10369	10351	22.9
Z12	$C_{768}H_{986}N_{48}O_{48}Zn_{12}$	12443	12416	22.5
Z16	$C_{1024}H_{1314}N_{64}O_{64}Zn_{16}$	16590	16566	21.8
Z20	$C_{1280}H_{1642}N_{80}O_{80}Zn_{20}$	20736	20769	21.2
Z24	$C_{1536}H_{1970}N_{96}O_{96}Zn_{24}$	24884	24465	20.7
Z32	$C_{2048}H_{2626}N_{128}O_{128}Zn_{32}$	33178	33292	19.9
Z40	$C_{2560}H_{3282}N_{160}O_{160}Zn_{40}$	41470	41177	19.2
Z48	$C_{3072}H_{3938}N_{192}O_{192}Zn_{48}$	49764	49497	18.7
Z64	$C_{4096}H_{5250}N_{256}O_{256}Zn_{64}$	66350	66323	17.8
Z96	$C_{6144}H_{7874}N_{384}O_{384}Zn_{96}$	99527	99050	16.8
Z128	$C_{8192}H_{10498}N_{512}O_{512}Zn_{128}$	132709	130295	16.1
Z192	$C_{12288}H_{15746}N_{768}O_{768}Zn_{192}$	199052	n.d.[d]	15.3
Z256	$C_{16384}H_{20994}N_{1024}O_{1024}Zn_{256}$	265416	n.d.	14.8
Z384	$C_{24576}H_{31490}N_{1536}O_{1536}Zn_{384}$	398122	n.d.	14.1
Z512	$C_{32768}H_{41986}N_{2048}O_{2048}Zn_{512}$	530830	n.d.	13.6
Z768	$C_{49152}H_{62978}N_{3072}O_{3072}Zn_{768}$	796242	n.d.	n.d.
Z1024	$C_{65536}H_{83970}N_{4096}O_{4096}Zn_{1024}$	1061658	n.d.	n.d.

[a] Calculated molecular weight. [b] Observed molecular weight detected by MALDI-TOF mass spectroscopy. [c] GPC-HPLC analysis (JAIGEL-5H-AF, 4H-AF, and 3H-AF columns in series). [d] n.d. = not determined.

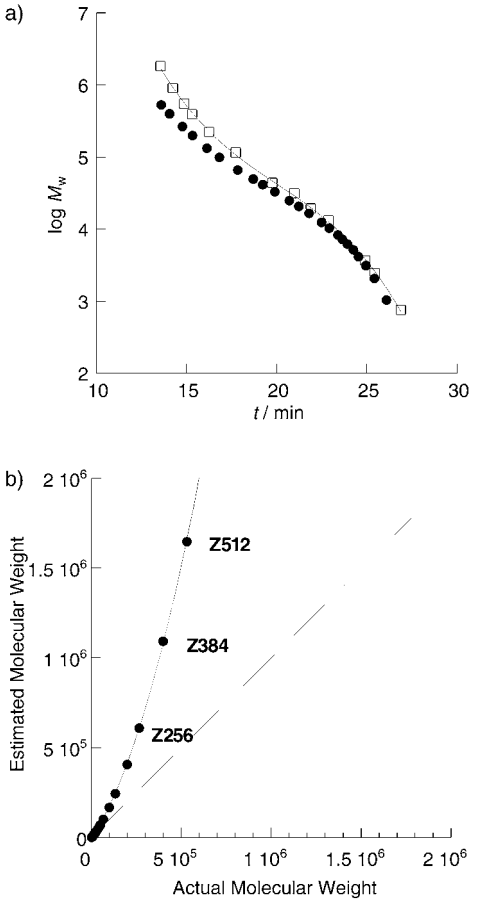

Figure 5. a) Relationship of the retention time versus log M_W for **Z*n*** (●) and standard polystyrene (□). b) The estimated molecular weights (number-average, M_n), determined by GPC, versus actual molecular weights of **Z*n*** (data points) relative to polystyrene standards (dashed line).

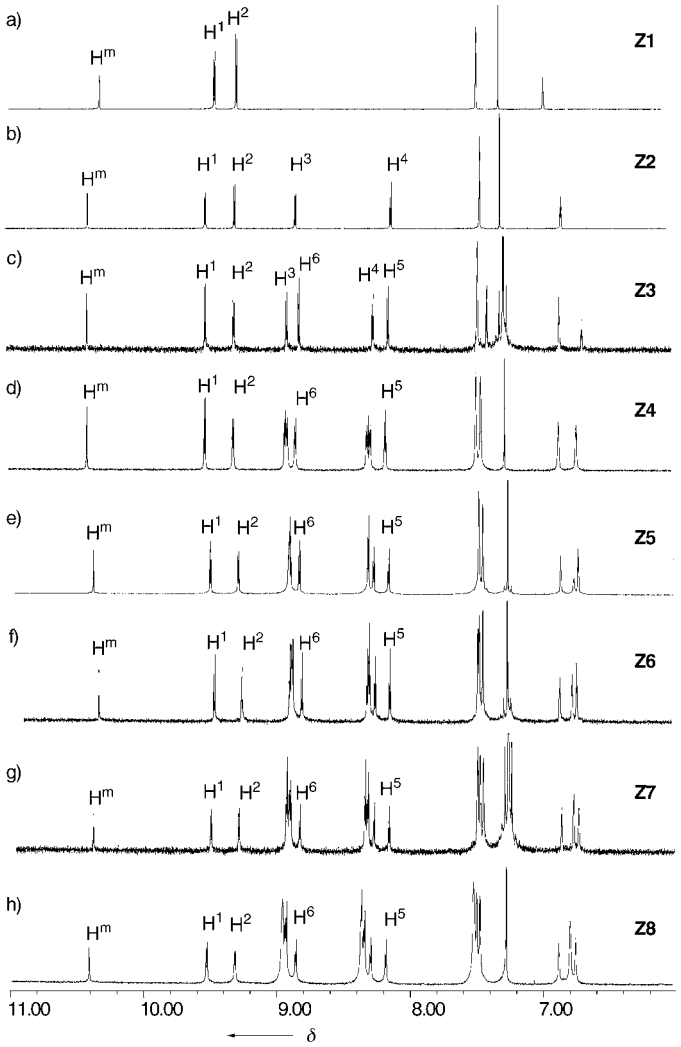

Figure 6. a)–h) ^{1}H NMR spectra, in $CDCl_3$, of **Z1**–**Z8**, respectively.

blets for the inner β protons H^3, H^4, H^5, and H^6. The ^{1}H NMR spectra of **Z1**–**Z8** clearly indicate totally symmetric structures with straight, rodlike conformations. The ^{1}H NMR spectra of **Z16**, **Z32**, **Z64**, and **Z128**, taken in $CDCl_3$ at room temperature, were shown in the previous

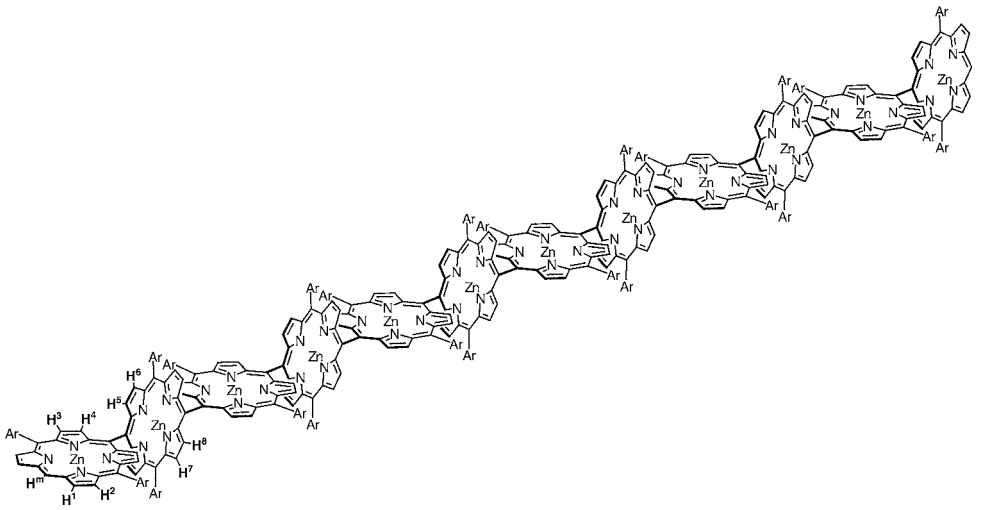

Scheme 3. Structure of **Z12** and proton designation. Ar = 3,5-dioctyloxyphenyl.

paper.[20b] Similar to these, the array **Z256** also displays a relatively well-resolved ^{1}H NMR spectrum, in which H^m appears as a singlet at 10.42 ppm, and H^1 and H^2 appear as two doublets at 9.53 and 9.31 ppm, respectively (Figure 7). It

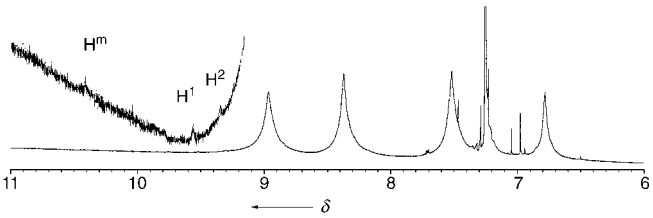

Figure 7. ^{1}H NMR spectrum of **Z256** in $CDCl_3$.

is noteworthy that H^m, H^1, H^2, and many inner β protons (H^3–H^8, etc.) appear at nearly the same chemical shifts for all the arrays, independent of concentration, indicating no significant aggregation of the arrays under these rather concentrated ^{1}H NMR conditions. The free-base porphyrin arrays **H*n*** show similar ^{1}H NMR spectra. The inner NH protons of the porphyrin appear at −3.15 ppm for **H1**, −2.44 ppm for **H2**, −1.65 (2H) and −2.40 ppm (4H) for **H3**, −1.62 (4H) and −2.39 ppm (4H) for **H4**, and −1.57 (4H), −1.60 (4H), and −2.38 ppm (4H) for **H6**. Thus, the signals of those inner protons are shifted to lower field, reflecting the ring current of neighboring and other close porphyrins (Supporting Information).

Single-crystal X-ray diffraction analysis: The molecular structure of 5,15-bis(3,5-dioctyloxyphenyl)porphyrin **H1** was determined by X-ray crystal analysis (Figure 8). The porphyrin rings show rather planar structures with small deviations (0.023 Å) from the mean planes, which consist of 24 core atoms. Single crystals of **Z2** were obtained from a THF/2-propanol solution, although unfortunately the diffraction data was not suitable for analysis (not shown).[29] Through many attempts to make single crystals of *meso*–*meso*-coupled porphyrin arrays, single crystals suitable for X-ray structure analysis were obtained for triporphyrin **Z$_P$3** (all aryl substituents of the porphyrin array were phenyl groups), which was the first crystal structure of a *meso*–*meso*-linked triporphyrin (Figure 9).[34] In the solid state, triporphyrin **Z$_P$3** displays a straight and orthogonal structure, with dihedral angles between the directly linked porphyrins of 88.3° and *meso*–*meso* bond lengths of 1.50(2) Å. This bond length is within the range of a typical C−C single bond.

The packing structures provide information on molecular interactions in the solid state. In the crystal structure of **H1**, both faces of each porphyrin are covered by the octyloxy side chains of the neighboring porphyrins in a parallel manner with a distance between carbon atoms and porphyrin plane of about 3.5 Å (Figure 8b). Interestingly, the noninteracting octyloxy side chains on the opposite side take an oblique orientation with respect to the porphyrin plane.

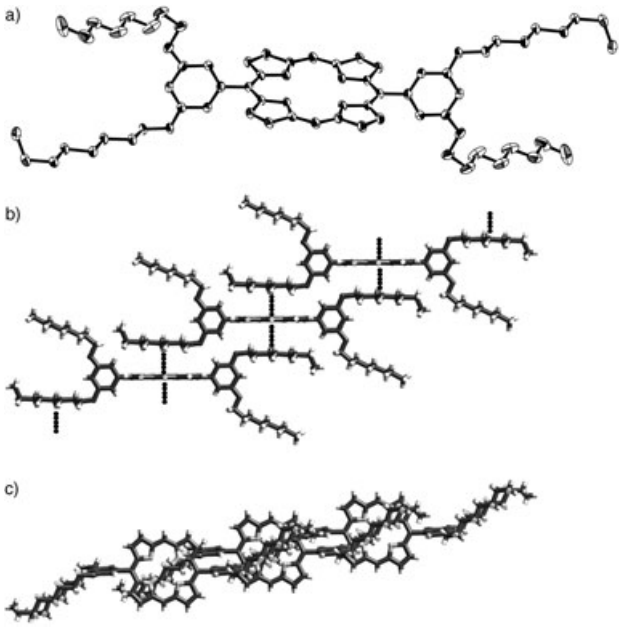

Figure 8. Crystal structure of **H1**. a) The ORTEP drawing with thermal ellipsoids at 50% probability. Hydrogen atoms are omitted for clarity. Crystal packing structure: b) side view and c) top view.

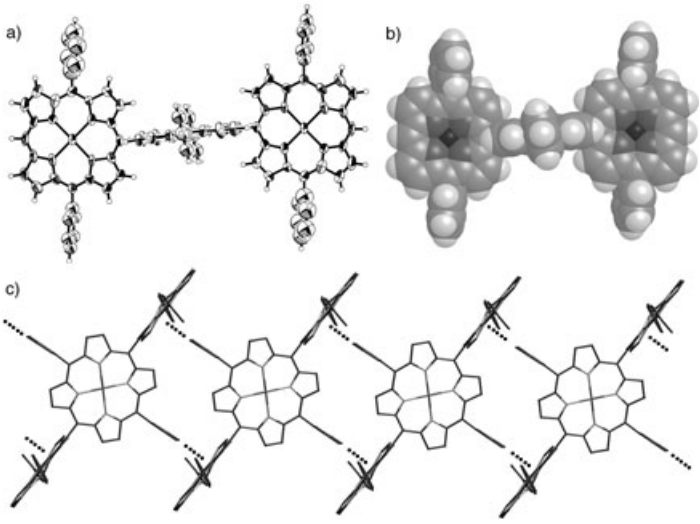

Figure 9. Crystal structure of **Z$_P$3**. a) The ORTEP drawing with thermal ellipsoids at 50% probability. Solvent molecules are omitted for clarity. b) The space-filling drawing. c) The crystal packing structure.

These structural features suggest a weak CH–π interaction between the porphyrin π plane and the parallel octyloxy side chain; this interaction leads to the formation of an infinite, one-dimensional network (Figure 8c). On the other hand, the porphyrin trimer **Z$_P$3** possesses a one-dimensional network with different structural motifs; orthogonally linked triporphyrin subunits are nicely packed, with weak CH–π interactions between the porphyrin π plane and the aromatic CH group.[31] The distance between the mean π plane and the phenyl *p*-carbon atom is estimated to be about 3.23 Å

(Figure 9c). This CH–π network structure cannot be suitable for **Z*n*** owing to *m*-dioctyloxy side chains.

Electrochemical properties: The one-electron oxidation potentials of the *meso–meso*-linked Zn^{II}–porphyrin arrays are also an important functional parameter for them, as well as for an understanding of the mechanism of the Ag^{I}-promoted *meso–meso* coupling.[32] Therefore, the electrochemical properties, particularly the one-electron oxidation potentials, were studied by cyclic voltammetry (CV) in dry $CHCl_3$ containing 0.1 M tetrabutylammonium tetrafluoroborate (nBu$_4$NBF$_4$) as a supporting electrolyte. At the time, we could not precisely measure waves associated with electrochemical reduction. The cyclic voltammograms of the Zn^{II}–porphyrin arrays are shown in Figure 10. The monomer **Z1** underwent a reversible first oxidation at 0.31 V (versus ferrocene/ferrocenium), while two reversible oxidation waves were detected in **Z2** at 0.28 and 0.43 V; these have been assigned as split first oxidation waves (one electron per porphyrin) judging from the results of other electronically coupled diporphyrins.[24b] This split one-electron oxidation for each Zn^{II}–porphyrin should arise from the influence of the positive charge of first-generated Zn^{II}–porphyrin radical cations. E_{OX1} of **Z2** was similar to that of **Z1**, indicating the

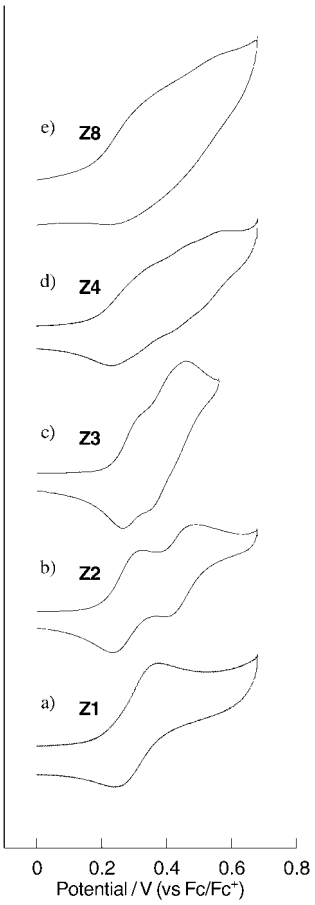

Figure 10. Cyclic voltammograms (vs Fc/Fc^+) for the oxidation of a)–d) **Z1**–**Z4**, respectively, and e) **Z8**, in $CHCl_3$ using a platinum working electrode and 0.1 M nBu$_4$NBF$_4$ as a supporting electrolyte.

HOMO in **Z2** is close to that in **Z1**, while E_{OX2} of **Z1** was slightly higher than its E_{OX1}. The one-electron oxidation potential of **Z3** was detected at 0.29 V, but the first oxidation potential waves of **Z4** and **Z8** could not be identified clearly. Despite the poorly resolved voltammograms, it was possible to assign the first one-electron oxidation at around 0.3 V for **Z4** and **Z8**. Therefore, it may be concluded that these Zn^{II}–porphyrin arrays (**Z*n***) have almost the same first one-electron oxidation potentials, which are independent of the number of porphyrin rings.

UV/Vis absorption and fluorescence spectroscopy: The optical properties of **Z*n***, up to **Z128**, were reported previously[23] and are summarized here. Characteristically, **Z*n*** exhibit large splitting of Soret bands due to strong exciton coupling. With an increase in the number of porphyrins, the low-energy Soret band is shifted to longer wavelengths, while the high-energy Soret band remains at nearly the same position, resulting in a progressive increase in the splitting energy. The observed Soret-band splitting can be described well by the exciton-coupling theory.[36] The energy difference between high- and low-energy Soret bands becomes larger as the array becomes longer, leading to an asymptotic feature ($\Delta E \cong 4615\ cm^{-1}$). On the other hand, the shifts in the Q bands are not so significant, but show a gradual increase in intensity. UV/Vis absorption spectra of **Z128**, **Z256,** and **Z512** are shown in Figure 11a. A plot of the molar extinction coefficients of **Z*n*** as a function of the number of porphyrin units exhibits a good linear correlation, indicating the higher absorptivity as the array becomes longer. In other words, each porphyrin moiety in the array acts as an independent light-absorbing unit.

On the other hand, the fluorescence quantum yields of **Z*n*** increase up to **Z16**, but then continuously decrease as the array becomes longer than **Z16**. The decreased fluorescence quantum yields of longer porphyrin arrays indicate that each porphyrin unit in the array cannot act as an individual fluorophore. As shown in Figure 11b, the total fluorescence intensity decreases from **Z128** to **Z256**, but not to such a great extent from **Z256** to **Z512**. The fluorescence decays of **Z*n*** also show a similar trend to the fluorescence quantum yields. As the porphyrin arrays become longer, their average fluorescence lifetimes decrease consistently up to **Z512**. In the arrays shorter than **Z16**, the fluorescence decays exhibit single exponential behavior. Conversely, as the array becomes longer than **Z16**, the fluorescence temporal profiles start to show double exponential decay, in which the contribution of the fast-decay component increases gradually with array length, up to **Z512** (Table 2). It should be noted that the fluorescence-decay profiles depend on the probe wavelength, especially in **Z256** and **Z512** (Supporting Information). Specifically, as the probe wavelength moves towards red, the overall fluorescence decay becomes slower in **Z256** and **Z512**. In shorter arrays, however, the fluorescence decays do not show this probe-wavelength dependence. This feature indicates that the excitation-energy migration occurs from the initially excited, shorter segments of

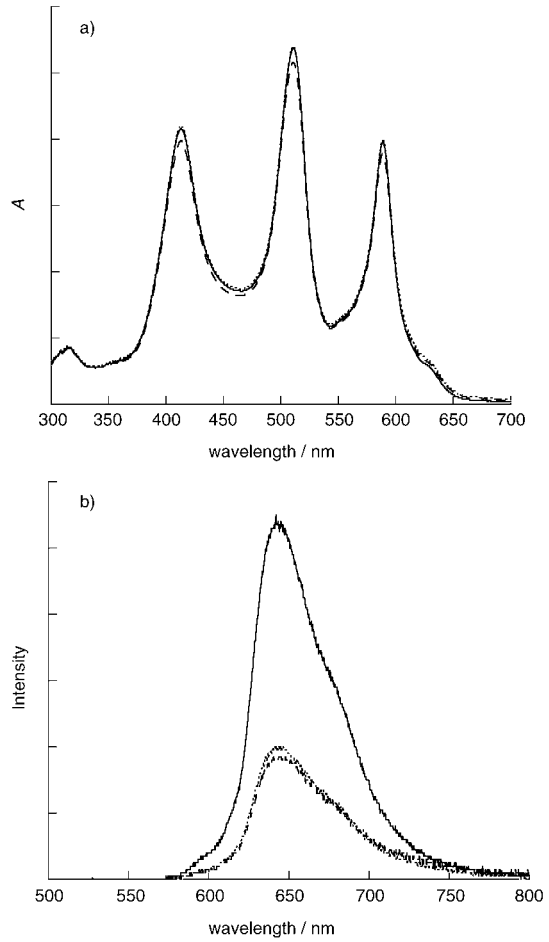

Figure 11. a) UV/Vis and b) fluorescence spectra of **Z128** (——), **Z256** (·····), and **Z512** (– – –) in THF.

Table 2. Fluorescence lifetimes of **Z*n***.[a]

	τ_1 [ns]	τ_2 [ns]	τ_{av} [ns]
Z1	–	–	2.62
Z2	–	–	1.83
Z3	–	–	1.72
Z4	–	–	1.65
Z6	–	–	1.59
Z8	–	–	1.55
Z12	–	–	1.52
Z16	–	–	1.50
Z24	1.49 (95.4)	0.14 (4.6)	1.43
Z32	1.48 (92.8)	0.33 (7.2)	1.40
Z48	1.47 (61.1)	0.08 (38.9)	0.93
Z64	1.47 (31.2)	0.08 (68.8)	0.51
Z96	1.45 (27.7)	0.14 (72.3)	0.50
Z128	1.42 (21.8)	0.22 (78.2)	0.49
Z256	1.05 (28.8)	0.14 (71.2)	0.40
Z512	0.92 (17.7)	0.12 (82.3)	0.26

[a] Numbers given in parentheses are percentages. τ_1, τ_2 are slow and fast decaying components of the fluorescence decay analyzed in terms of double exponential function, and τ_{av} is the averaged fluorescence lifetime.

porphyrin oligomer to the longer ones; this migration behavior is commonly observed in the photoexcitation dynamics of polymers.

The fluorescence excitation polarization of **Z1** was nearly 1/7 regardless of the excitation wavelength, which is typical when both absorption and emission oscillators are degenerate and polarized in the same plane.For **Z*n***, in contrast, negative anisotropy values were observed in the fluorescence excitation anisotropy spectra at around 413 nm, which corresponds to the high-energy Soret band, and positive anisotropy values were observed from 450 to 500 nm, which corresponds to the low-energy Soret band. The anisotropy values above ~450 nm for **Z*n*** became larger, reaching a maximum at **Z16,** and then decreased for the longer arrays. The maximum anisotropy value of ~0.3 above ~450 nm in **Z16**, which is still slightly smaller than 0.4 for perfect in-plane orientation between absorption and emission dipoles, indicates a nearly parallel alignment between absorption and emission dipoles upon photoexcitation at the low-energy exciton split Soret and Q bands. These features indicate that the overall geometries of **Z*n*** remain linear in form when **Z*n*** is shorter than **Z16** and thereafter start to deviate from linearity.

Conformational investigation by means of pulsed-field-gradient NMR (PFG-NMR) spectroscopy: To obtain information on the molecular motion of *meso–meso*-linked Zn^{II}–porphyrin arrays in solution, the self-diffusion coefficients (D) were measured based on pulsed-field-gradient NMR spectroscopy.[34,35] Usually D values become smaller (molecules diffuse more slowly) with increasing molecular size. Given that diffusion coefficients reflect effective hydrodynamic radii, not only the molecular size, but also the molecular shape will determine the value of D. Therefore, we may acquire information on the molecular shape of the porphyrin arrays in solution from their D values.

As noted above, all of these porphyrin arrays exhibit a singlet signal of H^m at around 10.4 ppm. Taking advantage of this ^{1}H-NMR characteristic signal, the D values (in $m^2 s^{-1}$) were determined on the basis of the PFG method at 20 °C in $CDCl_3$ and are as follows: 9.7×10^{-10} for **Z3**, 3.4×10^{-10} for **Z8**, 1.3×10^{-10} for **Z20**, and 1.2×10^{-10} for **Z24**. Thus, it is actually shown that the D values become smaller with increasing molecular length (Figure 12).

Structure investigation by scanning tunneling microscopy (STM) and atomic force microscopy (AFM): In recent years, the determination of molecular shape with a certain molecular size has become more and more feasible by means of scanning tunneling microscopy.[36–40] Even atomic force microscopy can be effective in resolving a molecular shape and/or packing pattern of a sufficiently big molecule.[40] Therefore, an STM micrograph of **Z6** adsorbed on a Cu(100) surface was taken; it shows an image of paired dots, having a constant spacing of about 2.00 ± 1.04 nm between the dots (Figure 13a).[39a] This observation was assigned to **Z6** having a bent conformation on the Cu surface with the Zn^{II}–porphyrin at each end, which were imaged strongly by STM, attached parallel to the metal surface. Here we report the STM images of **Z9**, **Z48**, and **Z128** on a

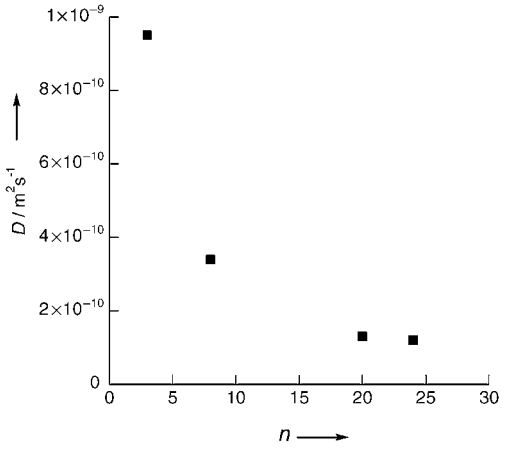

Figure 12. Diffusion coefficients of **Z3**, **Z8**, **Z20**, and **Z24** in $CDCl_3$. (n is the number of porphyrins.)

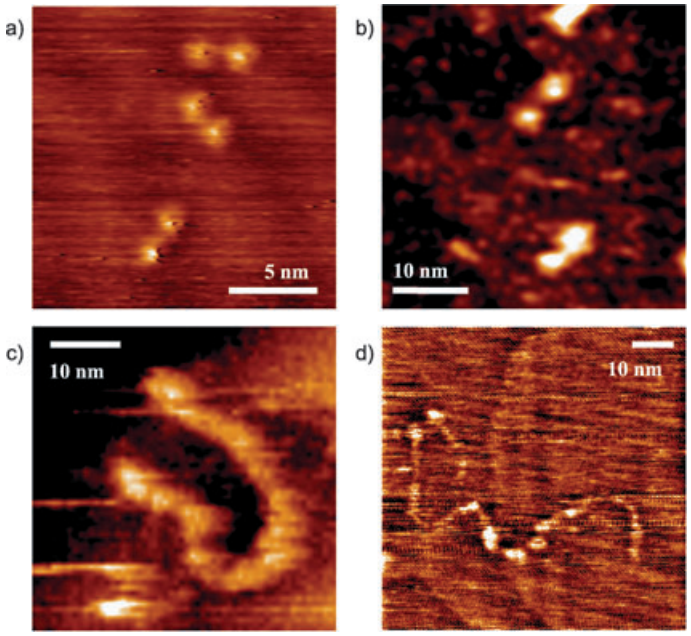

Figure 13. STM images of a) **Z6**, b) **Z9**, c) **Z48**, and d) **Z128**.

Cu(111) substrate. Sample deposition was performed using the pulse injection method under high vacuum (10^{-6} mbar).[41] The observed STM images are shown in Figure 13. As for **Z6**, the micrograph of the array **Z9**, which was taken at $V_s = 2.0$ V and $I = 0.03$ nA (V_s and I are sample bias voltage and tunneling current, respectively), shows a pair of images that are nearly constantly spaced at a distance of 55 Å (Figure 13b). As bright images usually stem from strong adsorption of π-conjugated molecules on a metal surface, the bright pair-based images seen here may be assigned to the adsorption of the two end porphyrins with their planes parallel to the metal substrate. Thus, it may be suggested that **Z9**, similar to **Z6**, takes a bent conformation with the porphyrins intermediate between the two end porphyrins being detached from the metal surface. This assignment suggests conformational flexibility of *meso–meso*-linked porphyrins. This feature is highlighted by the STM images of **Z48** and **Z128**. Among many unclear images that arose from significant entanglement or aggregation, a clear image of a single molecule of **Z48**, taken at $V_s = 2.0$ V and $I = 0.03$ nA, was obtained, which displays a severely bent conformation on the plane of the metal surface (Figure 13c). Significantly, the molecular length of **Z48** is estimated to be 43.5 nm from this STM image, which is exactly its predicted value. We also obtained a clear image of a single molecule of **Z128** (Figure 13d), taken at $V_s = 0.5$ V and $I = 0.05$ nA, which also shows a snakelike, largely bent structure with a molecular length of 117 nm that again agrees well with its predicted molecular length.

The detection of long porphyrin arrays on a single-molecule level has also been attempted by means of AFM on a highly oriented pyrolytic graphite (HOPG) substrate. In these experiments, a very dilute solution of porphyrin array in $CHCl_3$ was spread onto a freshly cleaved HOPG surface followed by slow evaporation of the solvent. Figures 14a and b displays the tapping-mode AFM images of **Z96**, in which the molecules are aligned along the graphite crystal lattice. It is interesting to note that many **Z96** molecules are observed with an extended-wire shape and with nearly the same molecular length of 87.3 ± 14.5 nm. Subsequently, single molecules of **Z256** and **Z512** were observed on a clean sapphire-Al_2O_3(0001) surface (Figures 14c and d, respectively). The single molecules were well dispersed and showed a clear zig-zag shape, with molecular lengths that were fully consistent with the structures. The molecular

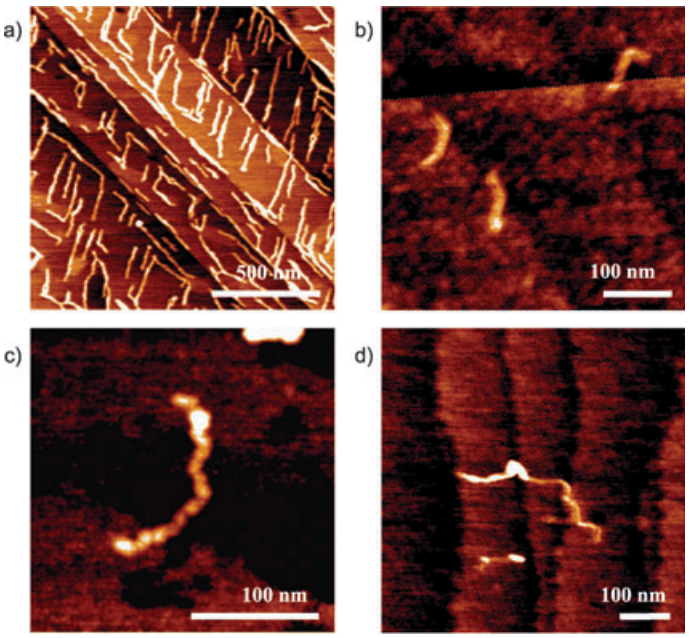

Figure 14. AFM images of a) **Z96** on HOPG, b) **Z96** on sapphire, c) **Z256** on sapphire, and d) **Z512** on sapphire.

lengths observed by scanning probe microscopy techniques versus the number of porphyrin units n are plotted in Figure 15.

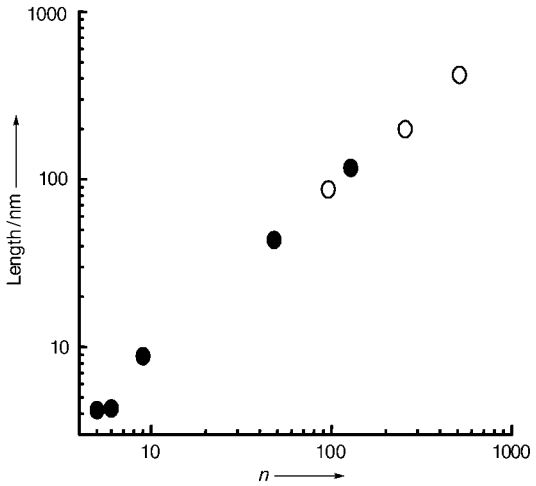

Figure 15. Relationship between the number of porphyrin units (n) and the observed molecular length, measured using AFM (○) or STM (●).

Fabrication of *meso–meso*-linked porphyrin arrays: Functionalization of one or both ends of the porphyrin array is the next important step for their useful application. When the fabrication of porphyrin arrays is possible with a thiol-containing group, resultant fabricated arrays could be used for covalent attachment on gold surfaces. For such a purpose, we selected Pd-catalyzed Suzuki–Miyaura arylation of *meso*-halogenated porphyrins with an arylboronic acid on the basis of several successful precedents.[42] However, usual thiol protective groups, such as acetyl and benzoyl groups, were found not to able to tolerate the basic conditions of the coupling reaction.[12,43] To avoid this, a diphenylmethyl group was selected as a protective group.[44] The synthesis of *meso*-thiophenylated porphyrin arrays is shown in Scheme 4. 4-Bromobenzenethiol (**8**) was protected with 1,1-diphenylmethanol (**7**) with the aid of trifluoroacetic acid (TFA) to form sulfide **9**, which was transformed into boronate **10** by a Pd-catalyzed reaction with an equivalent of bis(pinacolato)-diboron.[45]

Regioselective *meso,meso′*-dibromination of **Z2** was performed with 2.2 equiv *N*-bromosuccinimide (NBS) to give zinc(II)–*meso,meso′*-dibromoporphyrin $\mathbf{Z2Br_2}$ in quantitative yield. This bromination was similarly effective for **Z3**, **Z4**, **Z6**, **Z8**, **Z12**, **Z16**, **Z24**, **Z48**, and **Z64** to afford zinc(II)–*meso,meso′*-dibromoporphyrin arrays $\mathbf{Z3Br_2}$ (95%), $\mathbf{Z4Br_2}$ (87%), $\mathbf{Z6Br_2}$ (78%), $\mathbf{Z8Br_2}$ (83%), $\mathbf{Z12Br_2}$ (92%), $\mathbf{Z16Br_2}$ (84%), $\mathbf{Z24Br_2}$ (89%), $\mathbf{Z48Br_2}$ (91%), and $\mathbf{Z64Br_2}$ (87%), respectively, with high regioselectivity at the *meso*-position despite increasing pyrrolic β-positions in longer arrays, which are potentially susceptible to NBS bromination. The ratio of *meso*- to β-positions was as much as 256 in **Z64**. It is noteworthy that the present NBS bromination proceeded nearly quantitatively for all the $\mathbf{Zn}$ examined, which allowed for the isolation of pure $\mathbf{ZnBr_2}$ by passing the product through a short silica gel column without purification over a GPC column.

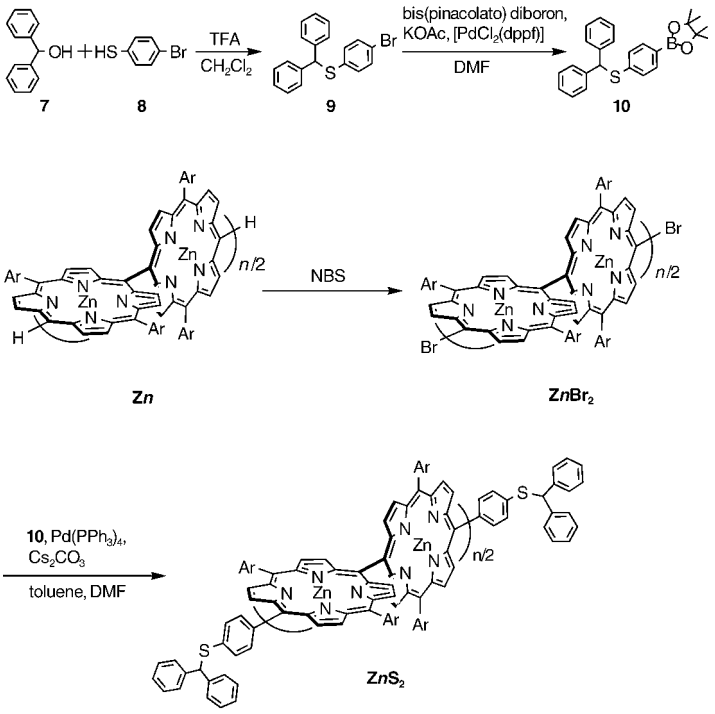

Scheme 4. Ar = 3,5-dioctyloxyphenyl.

Suzuki–Miyaura arylation of $\mathbf{Z6Br_2}$ with **10** (10 mol% Pd-$(PPh_3)_4$, 3 equiv Cs_2CO_3, DMF/toluene, at 90°C for 4 h) gave thiolated Zn^{II}–porphyrin array $\mathbf{Z6S_2}$ in 90% yield. Similarly, $\mathbf{Z12Br_2}$, $\mathbf{Z24Br_2}$, $\mathbf{Z48Br_2}$, and $\mathbf{Z64Br_2}$ were effectively arylated under the same conditions to furnish $\mathbf{Z12S_2}$ (85%), $\mathbf{Z24S_2}$ (79%), $\mathbf{Z48S_2}$ (81%), and $\mathbf{Z64S_2}$ (91%), respectively. Here again, the conversion of $\mathbf{ZnBr_2}$ to $\mathbf{ZnS_2}$ was nearly quantitative and almost-pure $\mathbf{ZnS_2}$ products were isolated by simple precipitation of the product. These products were also characterized by MALDI-TOF mass spectrometry and ^{1}H NMR spectroscopy. Figure 16 illustrates the comparison of the ^{1}H NMR spectra of **Z64**, $\mathbf{Z64Br_2}$, and $\mathbf{Z64S_2}$. The single H^m signal in the spectrum of **Z64** is missing in those of $\mathbf{Z64Br_2}$ and $\mathbf{Z64S_2}$, and the doublet signal for H^1 is low-field shifted in the spectrum of $\mathbf{Z64Br_2}$ due to the influence of the *meso*-substituted bromine, and high-field shifted in $\mathbf{Z64S_2}$ due to the influence of the *meso*-substituted aryl group. The protecting groups in $\mathbf{ZnS_2}$ can be cleaved by subjecting them to phenol/TFA (2.5% w/v) solution for a certain time to provide *meso,meso′*-phenylthiol-modified *meso–meso*-linked porphyrin arrays, the details of which will be reported elsewhere.

Discussion

The iterative dimerization strategy has proven to be effective for the preparation of very long *meso–meso*-linked Zn^{II}–porphyrin arrays. Although the same starting monomer

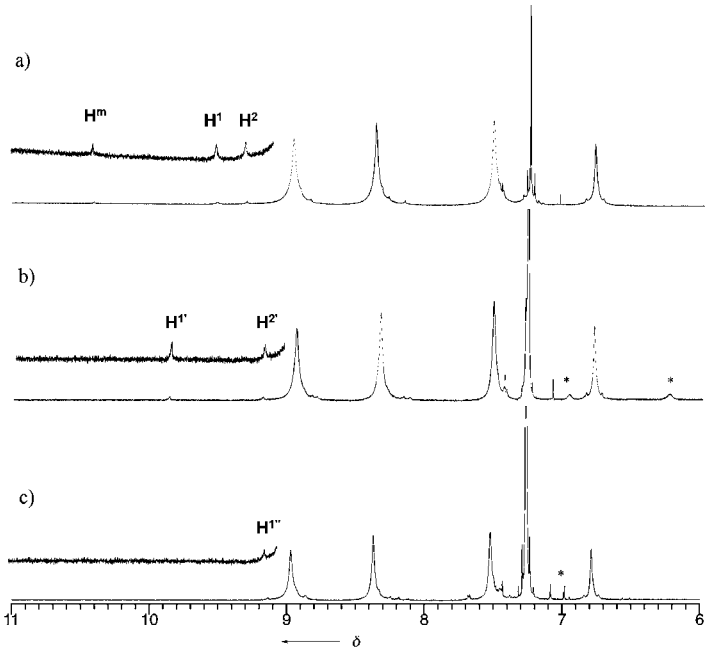

Figure 16. ^{1}H NMR spectra of a) **Z64**, b) **Z64Br$_2$**, and c) **Z64S$_2$** in $CDCl_3$.

Z1 can be polymerized to macromolecules with dispersed molecular weights under the slightly activated reaction conditions,[27] the stepwise doubling strategy, together with strict purification of each doubling product, allows for the discrete preparation of gigantically long molecules in an unprecedented manner. Crucial to this success is the high regioselectivity of the Ag^I-promoted oxidative coupling. In the reaction of ***Zn***, we did not observe the formation of any products that have any other form of connectivity. Equally important is the high solubility of ***Zn*** despite their large molecular weights; this solubility allows for the manipulation of these large molecules. We noted, however, marked differences in solubility and stability between the arrays up to **Z128** and those longer than **Z128**. As noted in the Results section, **Z128** can be stored for a long time without any serious chemical changes, while **Z256**, for example, tends to become insoluble when stored in the solid state for several months. This **Z256** solid is insoluble in organic solvents, precluding its analysis by GPC or UV/Vis spectroscopy. Another evident advantage of this doubling strategy is the large difference between the molecular weights of the reactant and products, which becomes larger as the reactant array becomes larger, thus making the separation of coupling products relatively easy over the preparative GPC-HPLC. Despite this advantage, the separation of extremely long molecules, such as **Z512** and **Z1024**, required multiple recycled separations over the GPC. Lastly, the long arrays, such as **Z128** and **Z256**, still have a self-coupling reactivity that is sufficient to produce even longer arrays in a reaction time comparable to those of the shorter arrays.

The high regioselectivity for *meso–meso* coupling observed for zinc(II)–5,15-diarylporphyrins may be related to its favorable a_{2u} HOMO. When a zinc(II)–5,10,15-triarylporphyrin is oxidized to its radical cation, the corresponding a_{2u} orbital becomes a magnetic orbital.[46] Such a radical cation will be attacked by a neutral Zn^{II}–porphyrin at its *meso*-position, which is, in this case, the most nucleophilic site. In line with this mechanism, the electrochemically generated radical cation of the zinc(II)–5,15-bis(3,5-di-*tert*-butylphenyl)porphyrin complex showed clear splitting in the ESR spectrum at $g=2.0055$, due to the coupling with the four porphyrinic nitrogen atoms ($a_N=1.5$ G), thus indicating that one electron was removed from the a_{2u} orbital (Supporting Information). A big question may be how two giant molecules can find two reacting sites (the end *meso*-positions) for each other in the reaction? Considering the large size of the porphyrin arrays, the coupling reaction must be entropically very unfavorable. Despite this, the coupling reactions proceed to give even longer products. One possible explanation may be the pre-association of porphyrin arrays in $CHCl_3$, which might bring two or more porphyrin arrays parallel to each other and their ends close together.

The ***Zn*** series is a rare example of a set of exactly discrete, homologous chain molecules covering a very wide range of molecular sizes (from 1000 to 1 000 000 Da). Thus, this series provides a nice opportunity to examine the relationship of hydrodynamic volume to molecular shape. As shown in Figure 5b, the molecular weights of ***Zn*** measured using polystyrene standards are much larger than the actual values. Particularly in the case of **Z512**, the estimated M_w is about three times larger than the actual M_w. This is in line with previous reports that the molecular weights of rodlike molecules,[17b,c,47] when estimated by GPC against random coil polystyrene standards, are considerably inflated relative to the actual values. These results thus indicate that ***Zn*** do not take random coil conformation like the polystyrene standards, but rather as a whole take rodlike conformation in solution. This relationship may provide important information on the hydrodynamic volume of one-dimensional rodlike molecules of molecular size up to $M_w=5\times10^5$ Da and is actually quite useful in estimating the weight-average molecular weights of large poly(porphyrinylene)s.[27]

Information on porphyrin arrays in solution may be gained from their self-diffusion coefficients (D). The Stokes–Einstein equation [Eq. (1)] relates D to the molecular parameters:

$$D = k_B T/f \quad (1)$$

where k_B is the Boltzmann constant, T is the absolute temperature, and f is the frictional coefficient, a measure of the forces that retard a molecule's motion. Equation (2) gives the expression for the frictional coefficient of a spherical particle:

$$f = 6\pi\eta r_H \quad (2)$$

where r_H is the hydrodynamic radius and η is the solvent viscosity. Equations (1) and (2) predict that the self-diffusion coefficient is inversely proportional to the hydrodynamic

radius. Interestingly, it has been predicted that Equation (2) can be used even for stiff, rodlike macromolecules by using Equation (3) to calculate r_H.

$$r_H = L/2[\ln(L/d)] \quad (3)$$

where L and d ($L \gg d$) are molecular length and diameter, respectively.[8] In the present case, the molecular length of **Z*n*** can be precisely predicted by the number of porphyrins, provided they have linear rodlike conformations in solution. Given $d = 10$ Å, their D values lead to an estimate of the effective L for **Z20** and **Z24** of 170 and 192 Å, respectively. These values are consistent with the calculated structures.

The rotational correlation time of the molecule (θ) is given by Equation (4):

$$\theta = \eta V/RT \quad (4)$$

where R is the gas constant, and V is the volume of the rotating unit. The rotational correlation time is also related to the diffusion coefficient by $\theta = (6D)^{-1}$. The rotational diffusion time, τ_{rot}, is the rotational correlation time per molecule and is therefore given by Equation (5):

$$\tau_{rot} = \eta V/k_B T \quad (5)$$

Because the rotational diffusion time can also be measured by the fluorescence anisotropy decay, we can obtain similar information about the self-diffusion processes of **Z*n*** in solution from PFG-NMR measurements. For longer arrays, slower fluorescence anisotropy decay times were observed,[23] mainly due to an increase in molecular hydrodynamic volume caused by an increase in the total length of **Z*n***.

A plot of the molecular extinction coefficient of **Z*n*** versus the number of porphyrins (n) indicated a linear summation behavior in absorption intensity as the arrays became longer. On the other hand, in arrays longer than **Z16**, the fluorescence quantum yield gradually decreased and the contribution by the short component became larger, exhibiting a good correlation with fluorescence quantum yield. This spectroscopic data has been ascribed to conformational heterogeneity in longer porphyrin arrays, and the degree of heterogeneity increases as the arrays become longer. These conformational heterogeneities are believed to arise from bending of the main chain, as well as dihedral angle distribution between adjacent porphyrin planes. On the whole, we may conclude that the *meso–meso*-linked porphyrin arrays take a roughly linear rodlike conformation despite substantial conformation flexibility and heterogeneity. Based on this, the observed change of freshly separated, long array samples to insoluble material may indicate possible entanglement of the main chain. Another explanation would be the usual aggregation-induced precipitation.

Achieving direct access to a single molecule has become a growing area of contemporary, interdisciplinary research since the discovery of STM in 1982.[36] Research in this area has also been aimed at the engineering of single molecules and/or atoms and at the exploration of molecular properties on an individual, nonstatistical basis. In 1996, an IBM research group succeeded in obtaining an image of a Cu^{II}–tetrakis-(3,5-di-*tert*-butylphenyl)porphyrin complex by means of STM.[37a] In recent years, this technique, combined with a suitable sampling method, has been applied to the imaging of large porphyrin oligomers.[38,39] Among the imaging methods, the pulse injection method under high vacuum[41] has been demonstrated to be particular effective in getting a good STM image of a large porphyrin array that is decomposed at high temperature (>300 °C). By employing this method, we succeeded in acquiring an STM image of **Z48** on a Cu(111) surface, which provided strong support for its discrete structure. However, its largely bent structure was somewhat unexpected, as a 10,20-*meso–meso* direct connection of porphyrins was thought to result in a stiffer, linear rodlike structure. A similarly bent and more winding structure was detected for **Z128** under comparable conditions. It is thus conceivable that conformation flexibility of **Z*n*** may be substantially large in solution and may become larger with increasing molecular size. The observed, roughly straight, structure of **Z96** on HOPG may stem from its favorable interaction with the graphite crystal lattice, hence suggesting that the conformational flexibility of porphyrin arrays depends on their environment.

Compared to the chain elongation steps, the purification issue is more serious for modifications of the porphyrin arrays. Separation of **Z*n*Br$_2$** from **Z*n*** was practically impossible over the preparative GPC because of the small difference in molecular weight of the products, and serious tailing of the long arrays on silica gel or alumina columns precluded the separation of these products. This obstacle has been circumvented by the quantitative NBS bromination of the array. This is also a remarkable finding, in that macromolecules in general tend to become less reactive upon increasing in size relative to small molecules. The NBS bromination proceeded in a quantitative manner at least up to **Z64**, in which there are only two free *meso*-positions versus 512 free pyrrolic β-positions that are all potentially susceptible to NBS bromination. Nevertheless, NBS bromination occurred exclusively only at both *meso*-positions, hence fabricating synthetic handles just at the edges of long, rodlike molecules. Furthermore, these **Z*n*Br$_2$** arrays have been quantitatively arylated with a boronate smoothly by means of a Pd-catalyzed Suzuki–Miyaura coupling reaction. These both-ends-manipulated porphyrin arrays will be quite useful in a variety of embryonic fields, including molecular-wire, sensor, and molecular electronics.

Conclusion

We have succeeded in synthesizing *meso–meso* directly linked zinc(II)–porphyrin arrays up to 1024-mer (**Z1024**) in a discrete manner by a repeated Ag^{I}–salt-promoted *meso–meso* coupling reaction. The arrays up to **Z128** are fully

characterized by ^{1}H NMR spectroscopy, MALDI-TOF mass spectrometry, and GPC-HPLC. The ^{1}H NMR spectrum of **Z256** was recorded, but its parent-ion peak could not be found in its MALDI-TOF mass spectrum. The actual molecular lengths of **Z48** and **Z128** were confirmed by STM, and those of **Z96**, **Z128**, **Z256**, and **Z512** were confirmed by AFM. We also succeeded in the manipulation of both ends of the porphyrin arrays through NBS bromination and subsequent Suzuki–Miyaura arylation (**Z*n*** to **Z*n*Br$_2$** to **Z*n*S$_2$**) up to the **Z64** series. In solution, the **Z*n*** arrays are considered to overall take linear rodlike structures, but with substantial conformational flexibility as judged from their ^{1}H NMR spectra, diffusion coefficients, eluting behavior on GPC-HPLC, and UV/Vis and fluorescence spectra. The conformational flexibility has been shown by STM images of single molecules on a Cu(111) surface and AFM images of single molecules on HOPG and Al_2O_3 surfaces. The chemistry described here reveals a new area for nanoscaled and sub-microscaled functional materials.

Experimental Section

General procedure: All reagents and solvents were of commercial reagent grade and were used without further purification except where noted. Dry CH_2Cl_2 and $CHCl_3$ were obtained by refluxing and distilling over CaH_2. ^{1}H NMR spectra were recorded on JEOL ALPHA-500 and ECA-600 spectrometers, and chemical shifts were reported in the delta scale relative to a $CHCl_3$ internal standard ($\delta = 7.26$ ppm). Spectroscopic-grade tetrahydrofuran (THF) and toluene were used as solvents for all experiments. UV/Vis absorption spectra were recorded on a Shimadzu UV-2400PC spectrometer. Steady-state fluorescence emission spectra were recorded on a Shimadzu RF-5300PC spectrometer. Mass spectra were recorded on a JEOL HX-110 spectrometer by means of the positive FAB ionization method with an accelerating voltage of 10 kV and a 3-nitrobenzyl alcohol matrix, or on a Shimadzu/KRATOS KOMPACT MALDI4 spectrometer by using the positive MALDI-TOF method with a 9-nitroanthracene matrix. Redox potentials were measured by cyclic voltammetry and differential pulse voltammetry on a BAS electrochemical analyzer (660 model). GPC-HPLC was performed by using a JASCO HPLC system with JAIGEL 2.5H-AF, 3H-AF, 4H-AF, and 5H-AF columns in series, and with a multiwavelength detector MD-915. Recycling preparative GPC-HPLC was carried out with a JAI LC-908 that used preparative JAIGEL-2.5H, 3H, 4H, and 5H columns. Preparative separations were performed by silica-gel flash column chromatography (Merck Kieselgel 60H Art.7736), silica-gel gravity column chromatography (Wako gel C-200), and preparative size-exclusion chromatography (BioRad Bio-Beads S-X1 packed in chloroform in a 4.0×100 cm HPLC column; flow rate 3.8 mL min^{-1}).

Single-crystal diffraction analysis: Data was collected on a Rigaku R-axis imaging plate refined by full-matrix least-squares procedures with anisotropic thermal parameters for the non-hydrogen atoms. The hydrogen atoms were calculated in ideal positions. Solutions of structures were performed by using the "Crystal Structure" crystallographic software package (Molecular Structure Corporation). Compound **H1** ($C_{64}H_{86}N_4O_4$): Crystals were obtained by vapor diffusion of EtOH into a CH_2Cl_2 solution of **H1**; a red-prism crystal of dimensions $0.7 \times 0.2 \times 0.1$ mm was used for calculations. Compound **Z$_p$3** ($C_{110}H_{66}N_{12}O_3Zn_3$): Crystals were obtained by vapor diffusion of MeOH into a CH_2Cl_2 solution of **Z$_p$3**; a red prism crystal of dimensions $0.2 \times 0.15 \times 0.1$ mm was used for calculations. The crystallographic details are summarized in Table 3. CCDC-261869 (**H1**) and CCDC-261870 (**Z$_p$3**) contain the supplementary crystallographic data for this paper. These data can be obtained free of charge from the Cambridge Crystallographic Data Centre via www.ccdc.cam.ac.uk/data_request/cif.

Table 3. Summary of crystallographic data for **H1** and **Z$_p$3**.

	H1	**Z$_p$3**
formula	$C_{64}H_{86}N_4O_4$	$C_{110}H_{66}N_{12}O_{12}Zn_3$
M_r	975.41	1943.94
crystal size [mm]	$0.7 \times 0.2 \times 0.1$	$0.2 \times 0.15 \times 0.10$
crystal system	triclinic	monoclinic
space group	$P\bar{1}$ (#2)	$P\bar{1}$ (#2)
a [Å]	9.150(4)	12.092(2)
b [Å]	11.801(8)	13.123(4)
c [Å]	13.869(7)	16.037(4)
α [°]	84.42(5)	78.27(1)
β [°]	74.47(4)	73.07(2)
γ [°]	76.70(4)	88.72(2)
V [Å^3]	1403(1)	2381.9(9)
ρ_{calcd} [g cm^{-3}]	1.154	1.355
Z	1	1
T [K]	123	123
no. of reflns	12808	11422
no. of unique reflns	6404	11422
variables	368	490
$\lambda_{MoK\alpha}$ [Å]	0.71073	0.71073
$2\theta_{max}$	55.0	55.0
GOF	1.091	1.113
max. peak [eÅ^{-3}]	0.30	1.29
min. peak [eÅ^{-3}]	−0.45	−0.99
$R1$ [$I > 3.0\sigma(I)$]	0.069	0.113
$wR2$ [$I > 3.0\sigma(I)$]	0.093	0.122

STM and AFM measurement conditions: For STM measurements Cu(100) or Cu(111) were used as substrates. Clean, flat surfaces of Cu(100) were obtained from a single crystal by Ar^+ sputtering and annealing (550 °C) cycles, while substrates of Cu(111) were made on a cleaved mica surface by thermal evaporation. The arrays were dissolved into the proper solvent ($CHCl_3$ or CH_2Cl_2) to an approximate concentration of 10^{-5} mol L^{-1}. They were deposited by spraying the solution (ca. 0.5 μL) onto the substrate under high vacuum (10^{-6} mbar) using the pulse injection method, which was adequate for the arrays too large to be thermally evaporated. STM imaging was performed in situ in constant-height mode at room temperature under ultra-high vacuum ($< 10^{-10}$ mbar), by using a home-built STM with an electrochemically etched Pt/Ir tip. For AFM measurements, the arrays were deposited by placing drops of a dilute solution of the array in $CHCl_3$ (ca. 10^{-5} mol L^{-1}) onto a tilted sapphire substrate (Al_2O_3(0001)) and leaving to air-dry under ambient conditions. AFM imaging was performed by using the intermittent-contact mode under ambient conditions with a commercially available AFM (Nanoscope III, Digital Instruments Ltd.) with Si cantilevers (resonant frequency $f = 300$ kHz).

Acknowledgements

This work was supported by CREST (Core Research for Evolutional Science and Technology) of the Japan Science and Technology Agency (JST). We thank Prof. T. Kato and Dr. K. Furukawa for taking the ESR measurements. N.A. thanks the JSPS Research Fellowship for Young Scientists and the Ogasawara Foundation for the Promotion of Science & Engineering.

[1] a) R. E. Martin, F. Diederich, *Angew. Chem.* **1999**, *111*, 1440; *Angew. Chem. Int. Ed.* **1999**, *38*, 1350; b) J. M. Tour, *Chem. Rev.* **1996**, *96*, 537; c) P. F. H. Schwab, M. D. Levin, J. Michl, *Chem. Rev.* **1999**, *99*, 1863; d) J. Cornil, D. Beljonne, J.-P. Calbert, J.-L. Brédas,

Adv. Mater. **2001**, *13*, 1053; e) A. Kraft, A. C. Grimsdale, A. B. Holmes, *Angew. Chem.* **1998**, *110*, 416; *Angew. Chem. Int. Ed.* **1998**, *37*, 402; f) J. S. Moore, *Acc. Chem. Res.* **1997**, *30*, 402; g) D. T. McQuade, A. E. Pullen, T. M. Swager, *Chem. Rev.* **2000**, *100*, 2537; h) M. D. Watson, A. Fechtenkötter, K. Müllen, *Chem. Rev.* **2001**, *101*, 1267; i) D. Zhao, J. S. Moore, *Chem. Commun.* **2003**, 807; j) W.-S. Li, D.-L. Jiang, T. Aida, *Angew. Chem.* **2004**, *116*, 3003; *Angew. Chem. Int. Ed.* **2004**, *43*, 2943.

[2] a) C. K. Chiang, C. R. Fincher, Jr., Y. W. Park, A. J. Heeger, H. Shirakawa, E. J. Louis, S. C. Gau, A. G. MacDiarmid, *Phys. Rev. Lett.* **1977**, *39*, 1098; b) M. D. McGehee, A. J. Heeger, *Adv. Mater.* **2000**, *12*, 1655; c) C. J. Brabec, N. S. Sariciftci, J. C. Hummelen, *Adv. Funct. Mater.* **2001**, *11*, 15.

[3] Z. Grubisic, P. Rempp, H. Benoit, *J. Polym. Sci. Part B Polym. Lett.* **1967**, *5*, 753.

[4] P. M. Kovacic, B. Jones, *Chem. Rev.* **1987**, *87*, 357.

[5] a) G. Wegner, *Angew. Chem.* **1981**, *93*, 352; *Angew. Chem. Int. Ed. Engl.* **1981**, *20*, 361; b) J. G. Speight, P. Kovacicand, F. W. Koch, *J. Macromol. Sci. Rev. Macromol. Chem.* **1971**, *C5*, 295.

[6] a) T. Yamamoto, *Bull. Chem. Soc. Jpn.* **1999**, *72*, 621; b) D. Fichou, in *Handbook of Oligo- and Polythiophenes*, Wiley-VCH, Weinheim, **1999**.

[7] J. M. Tour, *Adv. Mater.* **1994**, *6*, 190.

[8] H. Yamakawa, in *Modern Theory of Polymer Solutions*, Harper & Row, New York, **1971**.

[9] P. Liess, V. Hensel, A. D. Schlüter, *Liebigs Ann.* **1996**, 1037.

[10] V. Hensel, A. D. Schlüter, *Chem. Eur. J.* **1999**, *5*, 421.

[11] U. Stalmach, H. Kolshorn, I. Brehm, H. Meier, *Liebigs Ann.* **1996**, 1449.

[12] a) J. M. Tour, *Acc. Chem. Res.* **2000**, *33*, 791; b) L. Jones II, J. S. Schumm, J. M. Tour, *J. Org. Chem.* **1997**, *62*, 1388.

[13] S. Huang, J. M. Tour, *J. Org. Chem.* **1999**, *64*, 8898.

[14] A. Cravino, N. S. Sariciftci, *J. Mater. Chem.* **2002**, *12*, 1931.

[15] a) J. Roncali, *Acc. Chem. Res.* **2000**, *33*, 147; b) J. Roncali, *Chem. Rev.* **1997**, *97*, 173; c) I. Jestin, P. Frere, P. Blanchard, J. Roncali, *Angew. Chem.* **1998**, *110*, 990; *Angew. Chem. Int. Ed.* **1998**, *37*, 942.

[16] a) M. Tachibana, S. Tanaka, Y. Yamashita, K. Yoshizawa, *J. Phys. Chem. B* **2002**, *106*, 3549; b) S. Tanaka, Y. Yamashita, *Synth. Met.* **1995**, *69*, 599.

[17] a) T. Izumi, S. Kobashi, K. Takimiya, Y. Aso, T. Otsubo, *J. Am. Chem. Soc.* **2003**, *125*, 5286; b) T. Otsubo, Y. Aso, K. Takimiya, *Bull. Chem. Soc. Jpn.* **2001**, *74*, 1789; c) K. Inouchi, S. Kobashi, K. Takimiya, Y. Aso, T. Otsubo, *Org. Lett.* **2002**, *4*, 2533.

[18] a) M. R. Wasielewski, *Chem. Rev.* **1992**, *92*, 435; b) D. Gust, T. A. Moore, A. L. Moore, *Acc. Chem. Res.* **1993**, *26*, 198; c) D. Gust, T. A. Moore, A. L. Moore, *Acc. Chem. Res.* **2001**, *34*, 40; d) D. Holten, D. F. Bocian, J. S. Lindsey, *Acc. Chem. Res.* **2002**, *35*, 57; e) A. K. Burrell, D. L. Officer, P. G. Plieger, D. C. W. Reid, *Chem. Rev.* **2001**, *101*, 2751.

[19] a) E. K. L. Yeow, K. P. Ghiggino, J. N. H. Reek, M. J. Crossley, A. W. Bosman, A. P. H. J. Schenning, E. W. Meijer, *J. Phys. Chem. B* **2000**, *104*, 2596; b) M.-S. Choi, T. Aida, T. Yamazaki, I. Yamazaki, *Chem. Eur. J.* **2002**, *8*, 2668; c) O. Mongin, A. Schuwey, M.-A. Vallot, A. Gossauer, *Tetrahedron Lett.* **1999**, *40*, 8347; d) S. Anderson, H. L. Anderson, J. K. M. Sanders, *Acc. Chem. Res.* **1993**, *26*, 469; e) J. Li, A. Ambroise, S. I. Yang, J. R. Diers, J. Seth, C. R. Wack, D. F. Bocian, D. Holten, J. S. Lindsey, *J. Am. Chem. Soc.* **1999**, *121*, 8927; f) H. A. M. Biemans, A. E. Rowan, A. Verhoeven, P. Vanoppen, L. Latterini, J. Foekema, A. P. H. J. Schenning, E. W. Meijer, F. C. de Schryver, R. J. M. Nolte, *J. Am. Chem. Soc.* **1998**, *120*, 11054; g) K.-i. Sugiura, Y. Fujimoto, Y. Sakata, *Chem. Commun.* **2000**, 1105; h) H. S. Cho, H. Rhee, J. K. Song, C.-K. Min, M. Takase, N. Aratani, S. Cho, A. Osuka, T. Joo, D. Kim, *J. Am. Chem. Soc.* **2003**, *125*, 5849.

[20] For preliminary reports of this work, see a) A. Osuka, H. Shimidzu, *Angew. Chem.* **1997**, *109*, 93; *Angew. Chem. Int. Ed. Engl.* **1997**, *36*, 135; b) N. Aratani, A. Osuka, Y. H. Kim, D. H. Jeong, D. Kim, *Angew. Chem.* **2000**, *112*, 1517; *Angew. Chem. Int. Ed.* **2000**, *39*, 1458.

[21] For other examples of *meso–meso*-linked porphyrin arrays, see a) K. Susumu, T. Shimidzu, K. Tanaka, H. Segawa, *Tetrahedron Lett.* **1996**, *37*, 8399; b) R. G. Khoury, L. Jaquinod, K. M. Smith, *Chem. Commun.* **1997**, 1057; c) M. O. Senge, X. Feng, *Tetrahedron Lett.* **1999**, *40*, 4165; d) J. Wojaczynski, L. Latos-Grazynski, P. J. Chmielewski, P. Van Calcar, A. L. Balch, *Inorg. Chem.* **1999**, *38*, 3040; e) X. Shi, L. S. Liebeskind, *J. Org. Chem.* **2000**, *65*, 1655; f) K. Ogawa, Y. Kobuke, *Angew. Chem.* **2000**, *112*, 4236; *Angew. Chem. Int. Ed.* **2000**, *39*, 4070; g) H. Imahori, K. Tamaki, Y. Araki, Y. Sekiguchi, O. Ito, Y. Sakata, S. Fukuzumi, *J. Am. Chem. Soc.* **2002**, *124*, 5165; h) D. Bonifazi, F. Diederich, *Chem. Commun.* **2002**, 2178; i) M. A. Miller, R. K. Lammi, S. Prathapan, D. Holten, J. S. Lindsey, *J. Org. Chem.* **2000**, *65*, 6634; j) M. Ottonelli, *Synth. Met.* **2003**, *138*, 173.

[22] N. Aratani, H. S. Cho, T. K. Ahn, S. Cho, D. Kim, H. Sumi, A. Osuka, *J. Am. Chem. Soc.* **2003**, *125*, 9668.

[23] Y. H. Kim, D. H. Jeong, D. Kim, S. C. Jeoung, H. S. Cho, S. K. Kim, N. Aratani, A. Osuka, *J. Am. Chem. Soc.* **2001**, *123*, 76.

[24] a) A. Tsuda, H. Furuta, A. Osuka, *Angew. Chem.* **2000**, *112*, 2649; *Angew. Chem. Int. Ed.* **2000**, *39*, 2549; b) A. Tsuda, H. Furuta, A. Osuka, *J. Am. Chem. Soc.* **2001**, *123*, 10304; c) A. Tsuda, A. Osuka, *Science* **2001**, *293*, 79; d) H. S. Cho, D. H. Jeong, S. Cho, D. Kim, Y. Matsuzaki, K. Tanaka, A. Tsuda, A. Osuka, *J. Am. Chem. Soc.* **2002**, *124*, 14642.

[25] a) P. S. Crezy, G. A. Smith, *Aust. J. Chem.* **1969**, *22*, 239; b) Q. M. Wang, D. W. Bruce, *Synlett* **1995**, 1267; c) B. J. Littler, M. A. Miller, C.-H. Hung, R. W. Wagner, D. F. O'Shea, P. D. Boyle, J. S. Lindsey, *J. Org. Chem.* **1999**, *64*, 1391; d) T. E. O. Screen, K. B. Lawton, G. S. Wilson, N. Dolney, R. Ispasoiu, T. Goodson III, S. J. Martin, D. D. C. Bradley, H. L. Anderson, *J. Mater. Chem.* **2001**, *11*, 312; e) J.-W. Ka, C.-H. Lee, *Tetrahedron Lett.* **2000**, *41*, 4609.

[26] a) J. S. Lindsey, I. C. Schreiman, H. C. Hsu, P. C. Kearney, A. M. Marguerettaz, *J. Org. Chem.* **1987**, *52*, 827; b) S. G. DiMagno, V. S.-Y. Lin, M. J. Therien, *J. Org. Chem.* **1993**, *58*, 5983.

[27] N. Yoshida, N. Aratani, A. Osuka, *Chem. Commun.* **2000**, 197.

[28] A. Nakano, H. Shimidzu, A. Osuka, *Tetrahedron Lett.* **1998**, *39*, 9489.

[29] The X-ray crystal structure of *meso–meso*-linked Cu^{II}–diporphyrin was reported. N. Yoshida, T. Ishizuka, A. Osuka, D. H. Jeong, H. S. Cho, D. Kim, Y. Matsuzaki, A. Nagami, K. Tanaka, *Chem. Eur. J.* **2003**, *9*, 58.

[30] For other examples of X-ray crystal structures of singly, directly linked diporphyrins, see reference [21b] and a) Y. Deng, C. K. Chang, D. G. Nocera, *Angew. Chem.* **2000**, *112*, 1108; *Angew. Chem. Int. Ed.* **2000**, *39*, 1066; b) Y. Nakamura, N. Aratani, A. Tsuda, A. Osuka, K. Furukawa, T. Kato, *J. Porphyrins Phthalocyanines* **2003**, *7*, 264.

[31] a) B. Aurivillius, R. E. Carter, *J. Chem. Soc. Perkin Trans. 2* **1978**, 1033; b) M. Nishino, H. Hirota, *Tetrahedron* **1989**, *45*, 7201; c) H. Takahashi, S. Tsuboyama, Y. Umezawa, K. Honda, M. Nishio, *Tetrahedron* **2000**, *56*, 6185; d) M. Nishio, *CrystEngComm* **2004**, *6*, 130.

[32] a) T. Ogawa, Y. Nishimoto, N. Yoshida, N. Ono, A. Osuka, *Chem. Commun.* **1998**, 337; b) T. Ogawa, Y. Nishimoto, N. Yoshida, N. Ono, A. Osuka, *Angew. Chem.* **1999**, *111*, 140; *Angew. Chem. Int. Ed.* **1999**, *38*, 176.

[33] M. Kasha, *Rev. Mod. Phys.* **1959**, *31*, 162.

[34] C. S. Johnson, Jr., *Prog. Nucl. Magn. Reson. Spectrosc.* **1999**, *34*, 203.

[35] a) B. Olenyuk, M. D. Levin, J. A. Whiteford, J. E. Shield, P. J. Stang, *J. Am. Chem. Soc.* **1999**, *121*, 10434; b) W. H. Otto, M. H. Keefe, K. E. Splan, J. T. Hupp, C. K. Larive, *Inorg. Chem.* **2002**, *41*, 6172; c) W. S. Jeon, A. Y. Ziganshina, J. W. Lee, Y. H. Ko, J.-K. Kang, C. Lee, K. Kim, *Angew. Chem.* **2003**, *115*, 4231; *Angew. Chem. Int. Ed.* **2003**, *42*, 4097.

[36] G. Binnig, H. Rohrer, Ch. Gerber, E. Weibel, *Phys. Rev. Lett.* **1982**, *49*, 57.

[37] a) T. A. Jung, R. R. Schlittler, J. K. Gimzewski, H. Tang, C. Joachim, *Science* **1996**, *271*, 181; b) J. K. Gimzewski, C. Joachim, *Science* **1999**, *283*, 1683.

[38] a) H. L. Anderson, *Angew. Chem.* **2000**, *112*, 2552; *Angew. Chem. Int. Ed.* **2000**, *39*, 2451; b) N. Bampos, C. N. Woodburn, M. E. Welland, J. K. M. Sanders, *Angew. Chem.* **1999**, *111*, 2949; *Angew. Chem. Int. Ed.* **1999**, *38*, 2780; c) K.-i. Sugiura, H. Tanaka, T. Matsumoto, T. Kawai, Y. Sakata, *Chem. Lett.* **1999**, 1193; d) K.-i. Sugiura, T. Matsumoto, S. Ohkouchi, K. Naitoh, T. Kawai, Y. Takai, K. Ushiroda, Y. Sakata, *Chem. Commun.* **1999**, 1957.
[39] a) A. Takagi, Y. Yanagawa, A. Tsuda, N. Aratani, T. Matsumoto, A. Osuka, T. Kawai, *Chem. Commun.* **2003**, 2986; b) X. Peng, N. Aratani, A. Takagi, T. Matsumoto, T. Kawai, I.-W. Hwang, T. K. Ahn, D. Kim, A. Osuka, *J. Am. Chem. Soc.* **2004**, *126*, 4468.
[40] E. Mena-Osteritz, A. Meyer, B. M. W. Langeveld-Voss, R. A. J. Janssen, E. W. Meijer, P. Bäuerle, *Angew. Chem.* **2000**, *112*, 2791; *Angew. Chem. Int. Ed.* **2000**, *39*, 2679.
[41] H. Tanaka, T. Nakagawa, T. Kawai, *Surf. Sci.* **1996**, *364*, L575.
[42] a) X. Zhou, K. S. Chan, *J. Org. Chem.* **1998**, *63*, 99; b) D. A. Shultz, H. Lee, R. K. Kumar, K. P. Gwaltney, *J. Org. Chem.* **1999**, *64*, 9124; c) T. Mizutani, K. Wada, S. Kitagawa, *J. Am. Chem. Soc.* **2001**, *123*, 6459; d) L. Yu, J. S. Lindsey, *Tetrahedron* **2001**, *57*, 9285; e) A. G. Hyslop, M. A. Kellett, P. M. Iovine, M. J. Therien, *J. Am. Chem. Soc.* **1998**, *120*, 12676; f) N. Aratani, A. Osuka, *Org. Lett.* **2001**, *3*, 4213.
[43] D. L. Pearson, J. M. Tour, *J. Org. Chem.* **1997**, *62*, 1376.
[44] I. Photaki, J. T. -Papadimitriou, C. Sakarellos, P. Mazarakis, L. Zervas, *J. Chem. Soc. C* **1970**, 2683.
[45] a) T. Ishiyama, M. Murata, N. Miyaura, *J. Org. Chem.* **1995**, *60*, 7508; b) M. Murata, S. Watanabe, Y. Masuda, *J. Org. Chem.* **1997**, *62*, 6458; c) M. Murata, T. Oyama, S. Watanabe, Y. Masuda, *J. Org. Chem.* **2000**, *65*, 164.
[46] M. Kamo, A. Tsuda, Y. Nakamura, N. Aratani, K. Furukawa, T. Kato, A. Osuka, *Org. Lett.* **2003**, *5*, 2079.
[47] a) D. L. Pearson, J. S. Schumm, J. M. Tour, *Macromolecules* **1994**, *27*, 2348; b) J. S. Schumm, D. L. Pearson, J. M. Tour, *Angew. Chem.* **1994**, *106*, 1445; *Angew. Chem. Int. Ed. Engl.* **1994**, *33*, 1360; c) N. Sumi, H. Nakanishi, S. Ueno, K. Takimiya, Y. Aso, T. Otsubo, *Bull. Chem. Soc. Jpn.* **2001**, *74*, 979.

Received: December 20, 2004
Published online: March 30, 2005